AGU PUBLICATIONS

Geophysical Research Letters

RESEARCH LETTER
10.1002/2015GL064042

Key Points:
- The Earth's geomagnetic field dip angle strongly affects the mesospheric *E* fields
- Thunderstorm upward electrodynamic coupling is stronger at low latitudes
- Low-latitude mesospheric thundercloud fields are stronger and laterally shifted

Correspondence to:
R. Kabirzadeh,
rasoulk@stanford.edu

Citation:
Kabirzadeh, R., N. G. Lehtinen, and U. S. Inan (2015), Latitudinal dependence of static mesospheric *E* fields above thunderstorms, *Geophys. Res. Lett.*, *42*, 4208–4215, doi:10.1002/2015GL064042.

Received 1 APR 2015
Accepted 29 APR 2015
Accepted article online 6 MAY 2015
Published online 26 MAY 2015

Latitudinal dependence of static mesospheric *E* fields above thunderstorms

R. Kabirzadeh[1], N. G. Lehtinen[1,2], and U. S. Inan[1,3]

[1]Department of Electrical Engineering, Stanford University, Stanford, California, USA, [2]Department of Physics and Technology, University of Bergen, Bergen, Norway, [3]Department of Electrical Engineering, Koç University, Istanbul, Turkey

Abstract Electrostatic fields generated by thunderclouds can significantly heat and modify the lower ionospheric electrons at altitudes of 70–80 km. These fields can map to higher altitudes along the geomagnetic field lines and have been proposed as the mechanism for generation of whistler ducts. Previous 2-D modeling of these fields have been limited to azimuthally symmetric cases which requires a vertical magnetic field. We have developed a 3-D model of the electrostatic thundercloud fields which allows the consideration of effects of the geomagnetic field dip angle on the mapping of the fields to high altitudes. The results show stronger electric fields at altitudes of 70–110 km with an equatorward and eastward shift of tens of kilometers at lower geomagnetic latitudes. These stronger fields are mapped into the magnetosphere and may therefore be important for whistler duct generation. The fields also indicate a more significant contribution of the quiescent heating on VLF early/fast events.

1. Introduction

The influence of thundercloud electrostatic and quasi-electrostatic fields at high altitudes (~60–150 km) has been the subject of numerous studies [see, for example, *Holzer and Saxon*, 1952; *Park and Dejnakarintra*, 1973; *Dejnakarintra and Park*, 1974; *Tzur and Roble*, 1985; *Pasko et al.*, 1995; *Inan et al.*, 1996; *Pasko et al.*, 1998; *Pulinets et al.*, 2000; *Tonev and Velinov*, 2005]. The fields are generated by charged particles created by various mechanisms in the thundercloud and distributed by updrafts within the cloud. The charging process takes place over many minutes and the fields created can thus be considered electrostatic. Lightning results in the sudden removal or redistribution of the thundercloud charges and can thus disturb the steady state conditions. These disturbances persist over a relatively long time scale and thus may be considered as quasi-electrostatic (QE). The quasi-electrostatic fields of lightning discharges at high altitudes and their role in generation of sprites and runaway electrons have also been the subject of many studies [*Lehtinen et al.*, 1996, 1997; *Pasko et al.*, 1997; *Qin et al.*, 2011, and references therein]. These phenomena are also influenced by the steady state conditions generated by the electrostatic fields before the lightning strike such as the quiescent heating of the ionospheric electrons [*Inan et al.*, 1996; *Pasko et al.*, 1998].

Based on the simple model of *Holzer and Saxon* [1952], there are three factors that increase penetration of thundercloud fields to ionospheric altitudes: (1) higher altitude of thundercloud charges, (2) larger magnitude of these charges, and (3) larger scale height of ambient conductivity profile. Due to very high specific conductivity, the electrostatic potential can map from the ionospheric *D* and *E* regions to higher altitudes along the geomagnetic field lines with very small attenuation. *Park and Helliwell* [1971] showed that transverse (i.e., perpendicular to the geomagnetic field) electric fields of 10 mV/m at 100 km altitude can create 5% field-aligned electron density variations at $L = 4$ in ~30 min, which can trap whistler waves. The same authors proposed thunderclouds as the source of this electric field. With a simple analytical model considering a single point charge inside the thundercloud at middle to high latitudes, *Park and Dejnakarintra* [1973] (hereafter referred to as PD73) calculated the transverse electric fields to be ~50 μV/m in the equatorial plane of the magnetosphere. They also considered the effects of anisotropies in the ionospheric conductivity for altitudes above ~70 km. Their calculations show that with anisotropic conductivities, i.e., taking into account the effect of the geomagnetic field, maximum radial electric field, E_r^{max}, is 3 orders of magnitude larger than that in the case of isotropic conductivity. Although PD73 model calculations considered a vertical geomagnetic field, the effects of these fields at lower latitudes are stronger since the attenuation of fields due to geomagnetic field line divergence when they are mapped to magnetosphere is stronger for higher latitudes [*Park and Helliwell*, 1971]. The model of PD73 has been since used by many others to study the thundercloud

electrostatic fields and their role in high altitudes chemistry and dynamics. *Vellinov and Tonev* [1994] improved the PD73 model for a thundercloud with multiple charge layers, by modeling the finite sizes of charges using a disk shape. They showed, as PD73 had predicted, that in most cases the relative contribution of the lowest positive charge for E_r in a thundercloud with three charge layers is negligible. *Vellinov and Tonev* [1994] further took into account electron production, loss, and advection and showed that the intense E_r can produce an electron hole above a thunderstorm of radius 50–100 km in the *E* and *F* regions. On the other hand, for an inverted dipole charge distribution, an electron density enhancement was created at the same heights. *Velinov and Tonev* [1995] further improved the previous models by using a piecewise exponential conductivity profile and found values of $E_r^{\max} = 10\mu$V/m at $z = 150$ km (for a charge $Q = 100$ C at $z_0 = 15$ km), which are about 2 orders of magnitude smaller than the values obtained by PD73.

Rodger et al. [1998a] tested the formulation of PD73 and confirmed it to be consistent with the experimental results of *Holzworth et al.* [1985]. The authors, however, suggested a much smaller upper (10–15 km) positive charge (7–8 C compared to 40–70 C suggested by *Holzworth et al.* [1985]) based on the model results and argued that the lower charge may be due to the screening charge layer above the top layer. Thundercloud electric fields at high altitudes and their possible role in whistler duct formation was also considered by *Rodger et al.* [1998b, 2002] and *McCormick et al.* [2002] with contradicting conclusions. Namely, *Rodger et al.* [1998b, 2002], using experimentally measured conductivity profiles of the atmosphere [*Hale*, 1984; *Holzworth et al.*, 1985], suggested that the fields can play an important role in the duct creation, while *McCormick et al.* [2002], using the same conductivity profiles and a more realistic charge structure, argued that the fields are not important.

Tonev and Velinov [2002] were the first to consider the effects of nonvertical geomagnetic field on the structure and strength of the electrostatic fields above a thunderstorm. They solved for the electrostatic fields at polar and equatorial latitudes (vertical and horizontal magnetic fields). At the equator, they reported an eastward horizontal shift of 3–100 km at 70–100 km altitude in the electric field structure, which increased with altitude. Their results, however, underestimated the experimental results found by *Holzworth et al.* [1985] by a factor of ~3. The authors explain the discrepancy by stating that "the model can not adequately reflect the modification of the thundercloud conductivity itself." The asymmetric structure and the shift of the electric field were later also predicted for the transient quasi-electrostatic fields following a lightning discharge [*Tonev and Velinov*, 2005].

Pasko et al. [1998] developed a cylindrically symmetric 2-D numerical model, self-consistently solving for conductivity changes by taking into account the electron heating. The electric field used was below breakdown threshold and thus no ionization effect was considered. Intense heating regions were predicted with lateral extent varying from 150 km to 350 km and the vertical extent of about 10 km covering most of the *D* region at 70–80 km which could extend to 85 km depending on the conductivity profile used. The heating effect on the specific conductivity, $\sigma_{\|}$, which controls the penetration of the vertical component of the electric field, is such that the conductivity in the lower part of *D* region is decreased but then sharply increases to ambient values at higher altitudes. The decrease of $\sigma_{\|}$ smooths out the vertical gradients, facilitating the upward penetration of the vertical electric fields. However, the sudden increase of conductivity, inhibits the penetration so that at 90 km the electric field is 70% lower than in the case without heating.

In this paper, a high-resolution three-dimensional electrostatic heating model is developed to determine the penetration of electric fields generated by a thundercloud into ionosphere. The model self-consistently considers *E*-field-driven electron heating, and the resulting conductivity changes and can include a realistic geomagnetic field. For this study we consider only the long time scale effects (minutes to hours) in the charge accumulation phase of the thundercloud.

2. Model

The model is based on the solutions of the quasi-electrostatic equations [*Pasko et al.*, 1998] in a three-dimensional Cartesian coordinate system. The axes are chosen so that $\hat{x}$ points to the magnetic east, $\hat{y}$ is in the meridian plane and points to the magnetic north, and $\hat{z}$ points to the zenith. The electrostatic potential ϕ in the simulation domain is found from charge conservation equation

$$\nabla \cdot \vec{J}_{\text{tot}} = \nabla \cdot (-\hat{\sigma}\nabla\phi + \vec{J}_s) = 0 \tag{1}$$

where the source $\vec{J}_s$ is the current density inside the thunderstorm responsible for the electrification of the cloud. The conductivity tensor, $\hat{\sigma}$, for a magnetic field in the *yz* plane is written as follows:

$$\hat{\sigma} = \begin{pmatrix} \sigma_P & \sigma_H S & \sigma_H C \\ -\sigma_H S & \sigma_P S^2 + \sigma_\parallel C^2 & (\sigma_P - \sigma_\parallel) SC \\ -\sigma_H C & (\sigma_P - \sigma_\parallel) SC & \sigma_P C^2 + \sigma_\parallel S^2 \end{pmatrix} \tag{2}$$

where $\sigma_\parallel$, σ_P, and σ_H are field-aligned, Pedersen, and Hall conductivities, respectively, and $S = \sin(I)$, $C = \cos(I)$ where I is the magnetic dip angle, i.e., the angle between the magnetic field and $\hat{y}$. The total conductivity tensor consists of both ion and electron conductivities, $\hat{\sigma} = \hat{\sigma}_e + \hat{\sigma}_i$. At altitudes below $z = 70$ km the ion-neutral and electron-neutral collision frequencies are much higher than the ions and electrons gyrofrequencies. Thus, ions and electrons can be considered as unmagnetized and the conductivity tensors are approximately diagonal. The model ion conductivities at these altitudes are constant in time during the simulation and are initialized to a profile obtained from previous experimental and modeling studies of atmospheric conductivities [*Hale*, 1984; *Holzworth et al.*, 1985; *Park and Helliwell*, 1971]. At higher altitudes, electron and ion conductivities can be expressed as $\sigma_{\parallel e,i} = |q_{e,i}|N_{e,i}\mu_{e,i}$, $\sigma_{Pe,i} = |q_{e,i}|N_{e,i}\mu_{e,i}(1 + \mu_{e,i}^2 B^2)^{-1}$, $\sigma_{He,i} = -q_{e,i}N_{e,i}\mu_{e,i}^2 B(1 + \mu_{e,i}^2 B^2)^{-1}$ where $q_{e,i}$ are the charges, $N_{e,i}$ are the number densities, and $\mu_{e,i} = e/(m_{e,i}\nu_{e,i})$ are the nonmagnetized mobilities for electrons and ions. We use a dipole-model geomagnetic field, $B = \left(B_0/R^3\right)\sqrt{1 + 3\sin^2\lambda}$, where R is the distance from the center of the Earth in Earth radii, λ is the geomagnetic latitude, and $B_0 = 3.06 \times 10^{-5}$ T. The electron mobility changes greatly with electric field and introduces nonlinear behavior into the calculations. The changes in the electron density due to ionization and attachment are neglected in this study since the calculated electric fields are well below the values at which the effect of these processes becomes appreciable [*Inan et al.*, 1996; *Pasko et al.*, 1998].

The second term in equation (1) may be expressed as $\nabla \cdot \vec{J}_s = -\rho_s \sigma_\parallel / \epsilon_0$ where ρ_s is the source charge density inside the thundercloud [*Pasko et al.*, 1998]. Equation (1) with a constant ρ_s is solved on a three-dimensional structured grid in the Cartesian coordinate system. In order to take the conductivity changes into account self-consistently, the equation is solved iteratively until the conductivities and electric fields converge to their final values as in *Pasko et al.* [1998], a process which usually takes only a few iterations. For the side boundaries we can use any combination of Dirichlet or Neumann boundary conditions (e.g., $\phi = 0$ or $\partial\phi/\partial x = 0$, respectively, at $x = \pm x_{max}$). At $z = 0$ the ground conductivity can be assumed as infinite for the electrostatic case and thus we can take $\phi = 0$. The choice of the boundary conditions at the top boundary, however, is more complicated. For example, Dirichlet ($\phi = 0$) condition may not be used because it amounts to "short-circuiting" the transverse *E* field, in which we are interested, in particular, for its role in the generation of the whistler ducts. One way to overcome this problem is to extend the boundary to the conjugate hemisphere. However, such an extension is computationally prohibitive. A better choice of the boundary conditions would be to assume that only the electric field component parallel to the *B* field (due to the very high parallel conductivities) is zero at the top boundary. This assumption is also consistent with satellite and rocket observations of the parallel DC electric fields in the topside ionosphere and the magnetosphere. With the choice of the magnetic field direction in the *yz* plane we can express this condition as follows:

$$\frac{\partial\phi}{\partial y}\cos I - \frac{\partial\phi}{\partial z}\sin I = 0 \tag{3}$$

Condition (3) is neither a Dirichlet nor a Neumann boundary condition, and the existence and uniqueness of the solution to (1) is not guaranteed. However, there has been at least one previous report of its use which has produced successful results [*Moelter et al.*, 1998]. Note that the condition reduces to a Neumann boundary condition for a vertical magnetic field. Although a rigorous mathematical proof of the existence of the solution with the above boundary condition is beyond the scope of this study, our analysis and results shown in the next section support the correctness of the solutions and indicates the validity of our assumptions. The choice of the top boundary as described by equation (3) is limited to higher altitudes above ~120 km where the parallel conductivity exceeds several orders of magnitude the conductivities across the magnetic field lines and the magnetic field lines can be considered as equipotential. This boundary condition might not be valid in the case of strong field-aligned currents like during a magnetospheric substorm. At the side boundaries, both Dirichlet and Neumann boundary conditions introduce an error of 5–10% in the solutions close to the boundary. Thus, to minimize the error in the region of interest, it is necessary to take the side boundaries

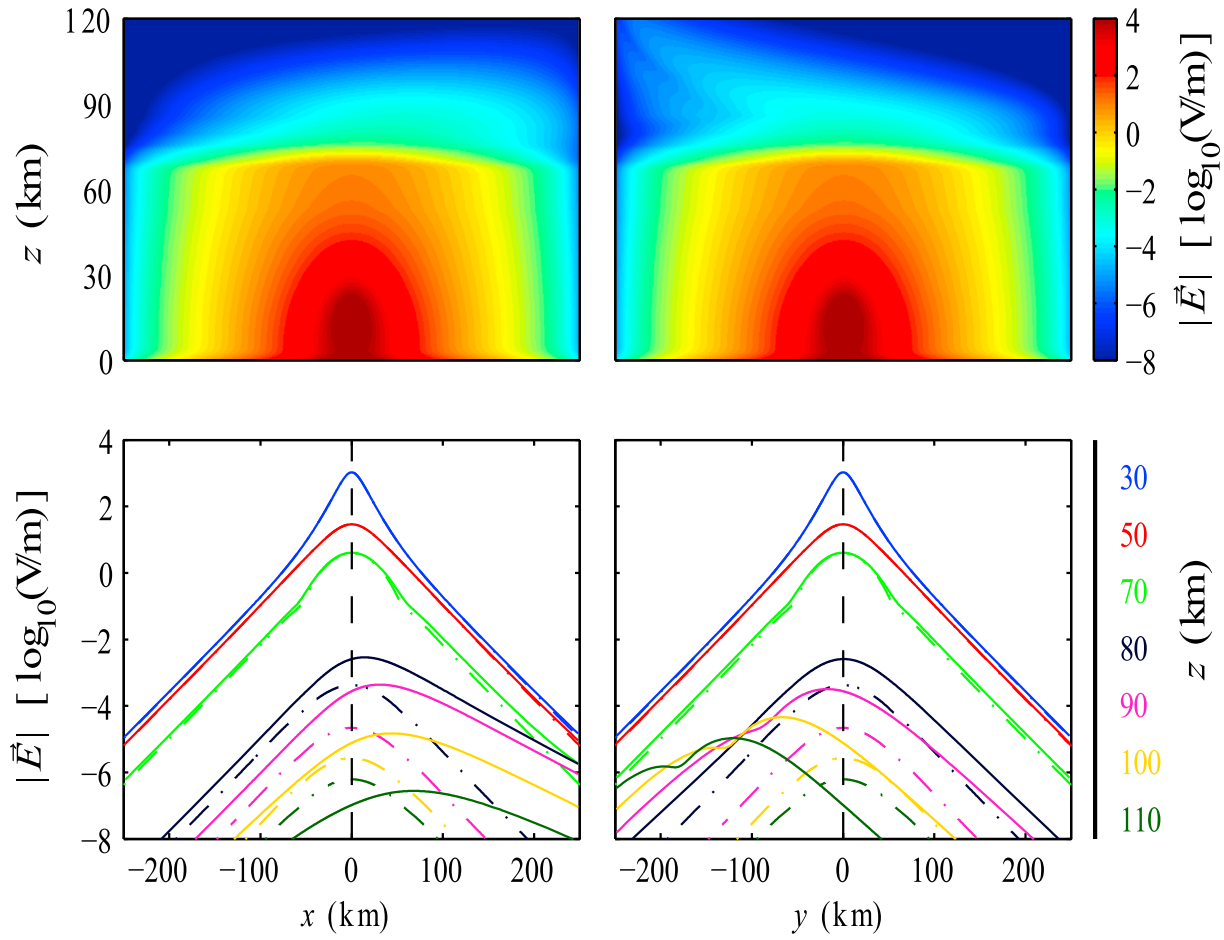

Figure 1. (top) Electrostatic fields at *xz* and *yz* planes passing from the center of charge distributions at low latitudes (dip angle $I = 10°$). (bottom) Electric field profiles at selected altitudes and the comparison between high-latitude ($I = 90°$, dash-dotted lines) and low-latitude (solid lines) fields.

at a far enough distance away from the center of the charge distributions. On the other hand, the spatial discretization of the equation (1) is second-order accurate and to minimize the error from the finite-difference approximation of the derivatives, a small spatial grid size (Δx, Δy, Δz) should be chosen. These two requirements dictate a very large number of grid points in each direction, which results in a very large system of discretized equations to be solved. In order to optimize the computer resources, we use a nonuniform coordinate system in the *x* and *y* directions, with a higher resolution in the region of interest, i.e., around the middle of the computational domain. To keep the second-order accuracy of the finite approximations we use the chain rule method for derivatives [*Moin*, 2010, Chapter 2, pp. 23–25]. Even when using nonuniform grids, the system of discretized equations is still too large to fit in the memory of a single computer, and even if enough memory is found, the limited processing power of a single computer would still not allow the calculation to be completed in a reasonable time. To overcome this problem, the model is parallelized using the domain-decomposition method for better performance, and the sparse system of difference equations is solved using High Performance Preconditioners package with generalized minimal residual solver with a semicoarsening multigrid preconditioner [*Falgout et al.*, 2006]. For the results shown in the next section we put the side boundaries 300 km away from the center of charge distributions and the top boundary at 200 km altitude. We discretize the domain with ($856 \times 856 \times 500$) points with a resolution of 339–8053 m depending on whether we are at the center of the domain or close to the side boundaries. The equations are solved with 56 processing cores on a cluster of computers each with 64 GB of memory and 12 processors.

3. Results

Figure 1 shows the magnitude of the electrostatic fields found from solving equation (1) on *xz* plane at $y = 0$ and *yz* plane at $x = 0$. The top row shows the field intensities on a logarithmic scale, and the bottom row displays the corresponding electric field profiles at selected altitudes represented by different colors. The results of the 2-D model which assumes a vertical geomagnetic field, are shown in the line plots as dash-dotted lines and the 3-D model results with a 10° magnetic dip angle are plotted as solid lines. To isolate the effect of the geomagnetic field direction, the system of source charges has been kept azimuthally symmetric, similar to the previous 2-D models. In other words, the upper thundercloud charge is assumed to be a Gaussian-distributed monopole charge of 100 C:

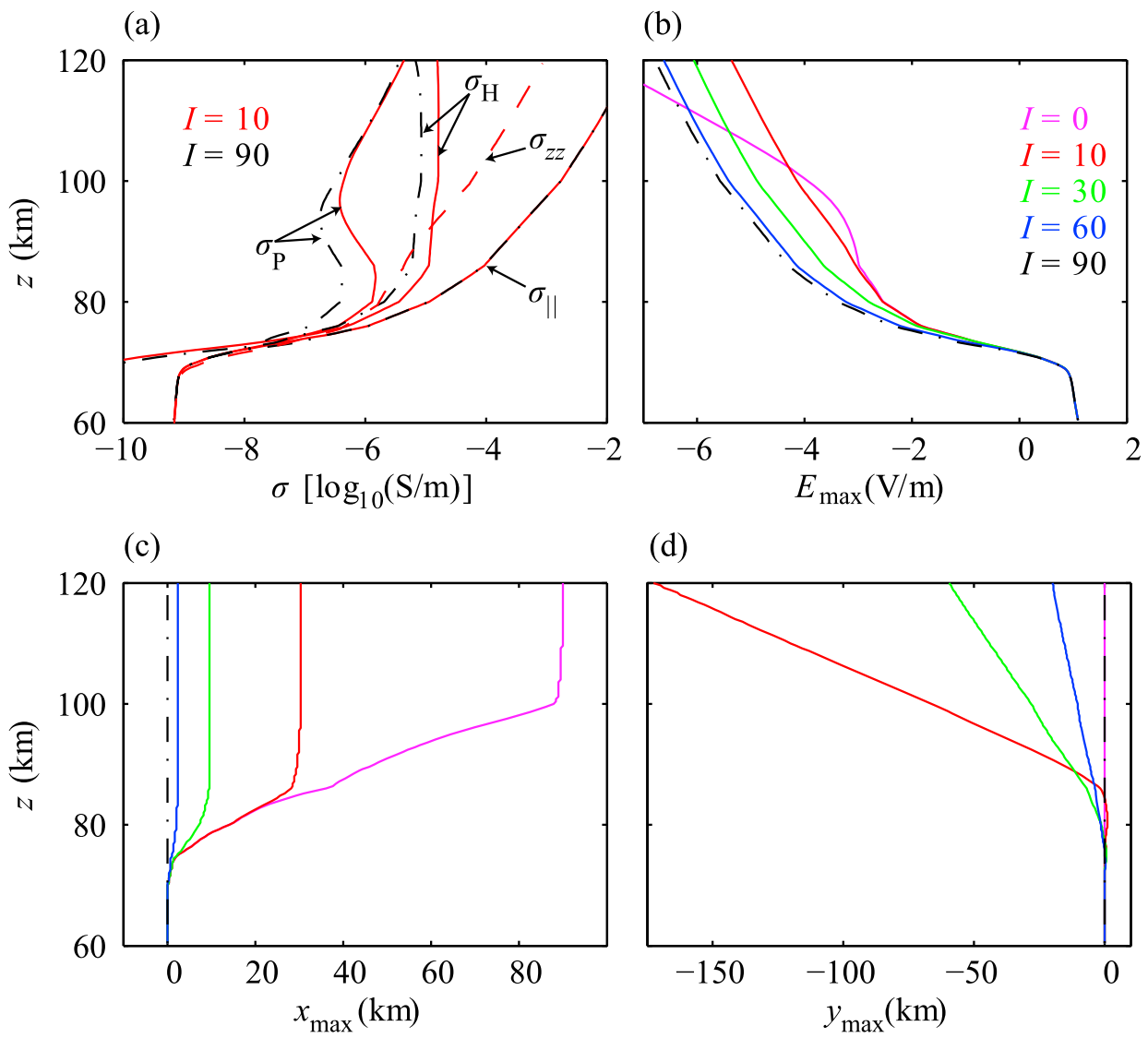

Figure 2. (a) The conductivity profiles at the location of E_{max}; (b) maximum electric field; (c) eastward shift of E_{max}; and (d) equatorial shift of E_{max}. The results shown are for 60–120 km altitude range for various magnetic dip angles.

$$\rho_s(x,y,z) = \rho_0 \exp\left[-\left(\frac{(x-x_0)^2}{a^2} + \frac{(y-y_0)^2}{b^2} + \frac{(z-z_0)^2}{c^2}\right)\right]$$

where $x_0 = 0$, $y_0 = 0$, $z_0 = 15$, $a = b = c = 3$ km.

The results shown in Figure 1 indicate that below ~70 km the fields are symmetric around the z axis and that there is very good agreement between the vertical and nonvertical magnetic field solutions at these altitudes. The medium there is nonmagnetized due to very high rates of collisions between the charged and the neutral particles and the geomagnetic field direction can thus be safely ignored. The 2-D model is thus sufficient at $z \lesssim 70$ km. At altitudes above ~70 km, however, the vertical and nonvertical geomagnetic field solutions start to deviate. The electric field structure at these altitudes are not axisymmetric and the peak electric fields are shifted in a horizontal direction. The shift in the $\hat{x}$ direction (eastward) is due to the low geomagnetic field dip angle ($I = 10°$ in this case). The electric field being mostly vertical, the large angle between $\vec{E}$ and $\vec{B}$ introduces the Hall currents in the $-\vec{E} \times \vec{B}$ direction. The peak electric fields are also displaced in the $-\hat{y}$ direction (southward). Further analysis of the solution of the fields in the Southern Hemisphere (not shown) shows a northward displacement therein. At the equator the electric field distribution becomes symmetric in the north-south direction at all altitudes. Thus, the north-south shift of the peak electric field is an equatorward shift in both hemispheres, which is larger at lower latitudes. This result can be explained by the fact that, due to very high ionospheric conductivity along the geomagnetic field lines, the electrostatic potential can map along the magnetic field lines with very low attenuation. At the equator, instead of the shift, we obtain symmetrical and slowly decaying electric field profiles in the north-south direction.

The self-consistent conductivity profiles at the location of maximum electric fields at altitudes of 60–120 km are shown in Figure 2a, where we compare the high-latitude (magnetic dip angle $I = 90°$) and low-latitude ($I = 10°$) profiles. The differences between these profiles are due both to the differences in the magnetic field strength and the nonlinear change of the electron mobility with electric fields. As mentioned in section 1, the scale height of the conductivity profile in the $\hat{z}$ direction, $\sigma_{zz} = \sigma_P \cos^2(I) + \sigma_{||} \sin^2(I)$, determines the strength

of the electric fields mapped to higher altitudes. For vertical geomagnetic fields at high latitudes, $\sigma_{zz} \simeq \sigma_{\parallel}$ and the conductivity parallel to the geomagnetic field lines maps the fields to higher altitudes. For low latitudes, however, the conductivity profile in the vertical direction is more complicated, as shown in Figure 2a for $I = 10°$ magnetic dip angle with the red dashed line. For altitudes below ~70 km, $\sigma_P \simeq \sigma_{\parallel}$ and thus $\sigma_{zz} \simeq \sigma_{\parallel}$. For altitudes between 70 and 85 km, σ_{zz} is controlled by both parallel and Pedersen conductivity terms. At higher altitudes the scaled parallel conductivity term dominates over the scaled Pedersen conductivity term, and $\sigma_{zz} \simeq \sigma_{\parallel} \sin^2(I)$. As can be seen from Figure 2a, for a nonvertical geomagnetic field, the vertical conductivity profile at altitudes higher than ~70 km has a larger scale height and hence the electric fields are mapped with less attenuation, which finds confirmation in the next panel. As shown in Figure 2b, the magnitude of the peak electric field is significantly (up to 2 orders of magnitude) larger at lower latitudes than at the high latitudes. The larger peak electric fields have significant implications for the mesospheric and thermospheric processes and indicate a stronger upward coupling between the electrified thunderstorms and the high-altitude space environment at middle to equatorial latitudes than previously believed. At the equator ($I = 0$), the parallel conductivity is completely horizontal and the electric field has to penetrate across the magnetic field lines to higher altitudes which becomes harder at higher altitudes since the ratio of $\sigma_P/\sigma_{\parallel}$ decreases with altitude.

Figures 2c and 2d show the horizontal location of the peak electric fields at altitudes of 60–120 km, for different magnetic dip angles. For nonvertical magnetic fields, the peak electric field starts to shift eastward above ~70 km altitude, and the shift linearly grows with altitude until it reaches its maximum, after which it remains constant. The altitude at which the fields reach their maximum eastward shift depends on the magnetic dip angle and is higher for smaller dip angles. The equatorward shift of the peak electric fields also starts above ~70 km, linearly grows with altitude, and is higher for lower dip angles. As discussed above, this result is consistent with the transverse electric field being efficiently "mapped" along the geomagnetic field lines. At the equator, the electric fields are symmetric in the north-south direction and the peak electric fields are not shifted in this direction.

4. Discussion

4.1. Whistler Duct Formation

The whistler duct formation mechanism proposed by *Park and Helliwell* [1971] needs strong transverse (i.e., perpendicular to the magnetic field lines) electric fields in order to create density irregularities in the average lifetime of a thunderstorm. The thundercloud-generated electrostatic fields are mainly vertical at all latitudes due to the configuration of the charges and the boundaries and the atmospheric conductivity gradient with height. At lower latitudes these vertical electric fields have a larger component perpendicular to the geomagnetic fields and may thus be more effective in the duct generation mechanism. Moreover, our analysis shows that by neglecting the direction of the geomagnetic fields at nonpolar latitudes, the *E* fields have until now been underestimated. The higher values of the fields at lower latitudes should favor the whistler duct generation mechanism proposed by *Park and Helliwell* [1971]. The transverse electrostatic fields at the nonpolar latitudes, unlike those used by *Park and Helliwell* [1971], are not symmetrical around the $\hat{z}$ axis. This asymmetry would impact the effectiveness of the fields and the spatial size and small-scale structures of the generated duct calculated from the *Park and Helliwell* [1971] theory. The detailed analysis of the effectiveness of the fields at nonpolar latitudes in the duct generation mechanism is beyond the scope of this paper.

4.2. Early/Fast Events

Electrostatic thundercloud fields have been proposed to persistently heat the ionospheric electrons to a quiescent level [*Inan et al.*, 1996]. Changes in the thundercloud charges by lightning discharges lead to heating/cooling above/below this quiescent level, which results in ionospheric modifications that can be seen as early/fast events in VLF waves propagating in the Earth-ionosphere waveguide. The calculated stronger electrostatic fields at nonpolar latitudes lead to a stronger level of heating above the thunderclouds and thus a larger ionospheric modification due to lightning discharges than previously estimated. These larger modifications may render the quiescent heating model more plausible [*Inan et al.*, 1996].

4.3. Implications for Sprites

As can be seen in Figure 2, the maximum electric fields at altitudes above ~70 km are larger than the maximum electric fields at the polar latitudes by up to 2 orders of magnitude. The electrostatic fields at lower latitudes also show an eastward and equatorward shift at altitudes higher than ~70 km. The eastward shift is

qualitatively consistent with the results of *Tonev and Velinov* [2002]. These shifts displace the heating region above the thundercloud horizontally. In addition to heating, the structured electric field configuration at lower latitudes might lead to significantly structured electron density distributions at altitudes where sprites and halos are produced. The electron density perturbation could be caused by electron convection or other chemical reactions neglected in this study which are important on long time scales comparable to the thundercloud charging time [*Gordillo-Vazquez*, 2008]. These preconditioning effects could be related to the observations of large-scale optical structures in the diffuse halos [*Moudry et al.*, 2003] and eventually lead to sprite initiation [*Qin et al.*, 2014].

Although the results presented here do not include the sprite-producing postdischarge quasi-electrostatic fields, *Tonev and Velinov* [2005] estimated a similar eastward shift for the postdischarge fields at equatorial regions. Their analysis, however, does not take into account the conductivity changes due to the electric fields self-consistently. Further self-consistent analysis of the postdischarge lightning quasi-electrostatic fields at nonpolar latitudes is needed to examine the effects of the magnetic field dip angle for these fields. In case the calculations of lightning-generated QE fields show a similar horizontal shift and stronger fields at high altitudes, the results would have extremely important implications on our understanding of the mechanisms responsible for the observations of horizontally displaced sprites [*Wescott et al.*, 2001; *São Sabbas et al.*, 2003] and the measurements and modeling of electric fields at the sprite initiation altitudes [*Hu et al.*, 2007].

Acknowledgments

This work was supported by Defense Advanced Research Projects Agency grant agreement HR0011-10-1-0058. We thank Morris Cohen and Robert Marshall for useful comments at various stages of the work. Requests for the data used for analysis and results can be directed to the corresponding author.

The Editor thanks two anonymous reviewers for their assistance in evaluating this paper.

References

Dejnakarintra, M., and C. Park (1974), Lightning-induced electric fields in the ionosphere, *J. Geophys. Res.*, *79*(13), 1903–1910, doi:10.1029/JA079i013p01903.

Falgout, R. D., J. E. Jones, and U. M. Yang (2006), The design and implementation of hypre, a library of parallel high performance preconditioners, in *Numerical Solution of Partial Differential Equations on Parallel Computers*, edited by A. M. Bruaset and A. Tveito, pp. 267–294, Springer, Berlin, Heidelberg, doi:10.1007/3-540-31619-1_8.

Gordillo-Vazquez, F. J. (2008), Air plasma kinetics under the influence of sprites, *J. Phys. D Appl. Phys.*, *41*(23), 234016, doi:10.1088/0022-3727/41/23/234016.

Hale, L. C. (1984), Middle atmosphere electrical structure, dynamics and coupling, *Adv. Space Res.*, *4*(4), 175–186, doi:10.1016/0273-1177(84)90283-7.

Holzer, R. E., and D. S. Saxon (1952), Distribution electrical conduction currents in the vicinity of thunderstorms, *J. Geophys. Res.*, *57*(2), 207–216, doi:10.1029/JZ057i002p00207.

Holzworth, R., M. Kelley, C. Siefring, L. Hale, and J. Mitchell (1985), Electrical measurements in the atmosphere and the ionosphere over an active thunderstorm: 2. Direct current electric fields and conductivity, *J. Geophys. Res.*, *90*(A10), 9824–9830, doi:10.1029/JA090iA10p09824.

Hu, W., S. Cummer, and W. Lyons (2007), Testing sprite initiation theory using lightning measurements and modeled electromagnetic fields, *J. Geophys. Res.*, *112*, D13115, doi:10.1029/2006JD007939.

Inan, U. S., V. P. Pasko, and T. F. Bell (1996), Sustained heating of the ionosphere above thunderstorms as evidenced in "early/fast" VLF events, *Geophys. Res. Lett.*, *23*(10), 1067–1070, doi:10.1029/96GL01360.

Lehtinen, N., M. Walt, U. Inan, T. Bell, and V. Pasko (1996), γ-ray emission produced by a relativistic beam of runaway electrons accelerated by quasi-electrostatic thundercloud fields, *Geophys. Res. Lett.*, *23*(19), 2645–2648, doi:10.1029/96GL02573.

Lehtinen, N. G., T. F. Bell, V. Pasko, and U. Inan (1997), A two-dimensional model of runaway electron beams driven by quasi-electrostatic thundercloud fields, *Geophys. Res. Lett.*, *24*(21), 2639–2642, doi:10.1029/97GL52738.

McCormick, R. J., C. J. Rodger, and N. R. Thomson (2002), Reconsidering the effectiveness of quasi-static thunderstorm electric fields for whistler duct formation, *J. Geophys. Res.*, *107*(A11), 1396, doi:10.1029/2001JA009219.

Moelter, M. J., J. Evans, G. Elliott, and M. Jackson (1998), Electric potential in the classical hall effect: An unusual boundary-value problem, *Am. J. Phys.*, *66*(8), 668–677, doi:10.1119/1.18931.

Moin, P. (2010), *Fundamentals of Engineering Numerical Analysis*, Cambridge Univ. Press, New York.

Moudry, D., H. Stenbaek-Nielsen, D. Sentman, and E. Wescott (2003), Imaging of elves, halos and sprite initiation at 1 ms time resolution, *J. Atmos. Sol. Terr. Phys.*, *65*(5), 509–518, doi:10.1016/S1364-6826(02)00323-1.

Park, C., and M. Dejnakarintra (1973), Penetration of thundercloud electric fields into the ionosphere and magnetosphere: 1. Middle and subauroral latitudes, *J. Geophys. Res.*, *78*(28), 6623–6633, doi:10.1029/JA078i028p06623.

Park, C., and R. Helliwell (1971), The formation by electric fields of field-aligned irregularities in the magnetosphere, *Radio Sci.*, *6*(2), 299–304, doi:10.1029/RS006i002p00299.

Pasko, V., U. Inan, T. Bell, and Y. N. Taranenko (1997), Sprites produced by quasi-electrostatic heating and ionization in the lower ionosphere, *J. Geophys. Res.*, *102*(A3), 4529–4561, doi:10.1029/96JA03528.

Pasko, V. P., U. S. Inan, Y. N. Taranenko, and T. F. Bell (1995), Heating, ionization and upward discharges in the mesosphere, due to intense quasi-electrostatic thundercloud fields, *Geophys. Res. Lett.*, *22*(4), 365–368, doi:10.1029/95GL00008.

Pasko, V. P., U. S. Inan, and T. F. Bell (1998), Ionospheric effects due to electrostatic thundercloud fields, *J. Atmos. Sol. Terr. Phys.*, *60*(7), 863–870, doi:10.1016/S1364-6826(98)00022-4.

Pulinets, S., K. Boyarchuk, V. Hegai, V. Kim, and A. Lomonosov (2000), Quasielectrostatic model of atmosphere-thermosphere-ionosphere coupling, *Adv. Space Res.*, *26*(8), 1209–1218, doi:10.1016/S0273-1177(99)01223-5.

Qin, J., S. Celestin, and V. P. Pasko (2011), On the inception of streamers from sprite halo events produced by lightning discharges with positive and negative polarity, *J. Geophys. Res.*, *116*, A06305, doi:10.1029/2010JA016366.

Qin, J., V. P. Pasko, M. G. McHarg, and H. C. Stenbaek-Nielsen (2014), Plasma irregularities in the D-region ionosphere in association with sprite streamer initiation, *Nat. Commun.*, *5*, 3740, doi:10.1038/ncomms4740.

Rodger, C. J., N. R. Thomson, and R. L. Dowden (1998a), Testing the formulation of Park and Dejnakarintra to calculate thunderstorm DC electric fields, *J. Geophys. Res.*, *103*(A2), 2171–2178, doi:10.1029/97JA02769.

Rodger, C. J., N. R. Thomson, and R. L. Dowden (1998b), Are whistler ducts created by thunderstorm electrostatic fields?, *J. Geophys. Res.*, *103*(A2), 2163–2169, doi:10.1029/97JA02927.
Rodger, C. J., N. R. Thomson, and R. L. Dowden (2002), Correction to "Are whistler ducts created by thunderstorm electrostatic fields?" by C. J. Rodger et al., *J. Geophys. Res.*, *107*(A6), 1068, doi:10.1029/2001JA009152.
São Sabbas, F. T., D. D. Sentman, E. M. Wescott, O. Pinto, O. Mendes, and M. J. Taylor (2003), Statistical analysis of space–time relationships between sprites and lightning, *J. Atmos. Sol. Terr. Phys.*, *65*(5), 525–535, doi:10.1016/S1364-6826(02)00326-7.
Tonev, P., and P. Velinov (2002), Electrostatic fields above thunderclouds at different latitudes and their ionospheric effects, *Adv. Space Res.*, *30*(11), 2625–2630, doi:10.1016/S0273-1177(02)80362-3.
Tonev, P., and P. Velinov (2005), Variations of quasi-electrostatic fields and ionosphere potential above lightning discharge at equatorial latitudes, *Adv. Space Res.*, *35*(8), 1461–1466, doi:10.1016/j.asr.2005.04.079.
Tzur, I., and R. Roble (1985), The interaction of a dipolar thunderstorm with its global electrical environment, *J. Geophys. Res.*, *90*(D4), 5989–5999, doi:10.1029/JD090iD04p05989.
Vellinov, P., and P. Tonev (1994), Penetration of multipole thundercloud electric fields into the ionosphere, *J. Atmos. Terr. Phys.*, *56*(3), 349–359, doi:10.1016/0021-9169(94)90216-X.
Velinov, P., and P. Tonev (1995), Modelling the penetration of thundercloud electric fields into the ionosphere, *J. Atmos. Terr. Phys.*, *57*(6), 687–694, doi:10.1016/0021-9169(94)E0016-G.
Wescott, E., H. Stenbaek-Nielsen, D. Sentman, M. Heavner, D. Moudry, and F. Sao Sabbas (2001), Triangulation of sprites, associated halos and their possible relation to causative lightning and micrometeors, *J. Geophys. Res.*, *106*(A6), 10,467–10,477, doi:10.1029/2000JA000182.